MSW MANAGEMENT -Multidisciplinary, Scientific Work and Management Journal
ISSN: 1053-7899
Vol. 36 Issue 2, 2026, Pages 1477-1484

IoT-Enabled Multi-Sensor Automatic Accident Detection and Alert System Using LabVIEW: Architecture, Implementation, and Performance Evaluation

G. Gopalakrishnan[1], Ellappan.V[2], Divakar M S[3], Hari Sankar K[4], Premkumar S[5]
[1]Assistant Professor, [2]Professor, [234]U.G Scholer — Department of Electronics and Communication Engineering, Mahendra Engineering College, Namakkal, Tamil Nadu, India
Mahendra Institute of Technology, Namakkal, Tamil Nadu, India
Corresponding Author: gopalkrishnangg@gmail.com , ellappan.v@gmail.com

ABSTRACT
Around 1.35 million people die in road traffic crashes globally every year, of which 50-70% are as a result of late responses to emergencies. In this paper, the design, implementation, and experimental validation of an Automatic Accident Detection and Alert System (AADAS) using the LabVIEW graphical system-design platform, which is based on Internet of Things (IoT) technology are presented. Coordinated by a microcontroller, Arduino Uno (ATmega328P), the system fuses information from five complementary sensors: ADXL335, a tri-axial MEMS accelerometer; MPU-6050, a six-DOF inertial measurement unit; SW-420, a vibration sensor; Hall-effect wheel-speed sensor; and MQ-3, a semiconductor alcohol sensor. There are 12 fundamental equations, which describe the physics of sensing, signal conditioning, decision logic for accidents, GPS positioning, and reliability of communications. A compound Boolean AND gate is used to separate the two cases (Normal and Accident) in LabVIEW. The ESP8266 Wi-Fi module transmits the message of the emergency alert via HTTP/MQTT within 2.5–4 seconds. It was validated experimentally in 120 controlled crash simulations with 97.2 % detection accuracy, less than 5 % false alarm, and a Packet Delivery Ratio (PDR) of 97.8 % at 35–40 % lower hardware cost than FPGA-based solutions.

Index Terms—IoT, Accident Detection, Multi-Sensor Fusion, LabVIEW, Arduino Uno, ADXL335, MPU-6050, SW-420, Hall-Effect Sensor, MQ-3, NEO-6M GPS, ESP8266, Intelligent Transportation Systems.

I. INTRODUCTION

Road traffic accidents (RTAs) are one of the major causes of avoidable deaths in the world and are highly demanding emergency response infrastructure. The first 60 minutes after an impact are known as the "golden hour" and deserve immediate medical attention to help save lives by over 70 % [1]. However, the incapacitation of the victims, coupled with the manual reporting process, makes it hard for this window of opportunity to be engaged in a large percentage of crashes. Technically, an embedded solution involving IoT systems that can automatically detect if a car has crashed, geolocate the crash, and send structured distress notifications in real-time is a viable solution to this gap. Although there is extensive prior work [1]–[15] there are four recurring limitations in the literature: (1) single parameter threshold detection, which can generate false alarms due to hard braking and road irregularities; (2) no structured and quantifiable percent based on anomaly detection; (3) high chip cost of FPGA-based implementations; and (4) no unified, low-cost platform for integrating reactive crash detection with proactive driver-condition monitoring. The proposed AADAS addresses all four limitations by the architecture and validated mathematical framework outlined in the following sections. The rest of this paper is structured as follows: In Section II, related work and research gaps are reviewed. In Section III, the proposed architecture of the system, twelve governing equations and implementation of LabVIEW software are described. Experimental Results and Comparative Analysis are given in Section IV. The paper is concluded in Section V.

II. RELATED WORK AND RESEARCH GAP ANALYSIS

Al-Shara [11] developed an accident detection system for GSM using a single impact threshold sensor, but reported false alarm rate more than 22 % which is caused by threshold ambiguity in hard brake condition. In order to enhance the accuracy of the motorcycle detectors, Basheer et al. [13] suggested a single-accelerometer motorcycle detector that only achieved 75–80 % accuracy due to the lack of multi-axis signal correlation. Hassan et al. [7] proposed a hybrid accelerometer-GSM configuration that was more accurate than the previous single-sensor-based configurations, but left out real-time waveform visualization and cross-parameter validation. The detection results of the ablation study presented in Table II of Section IV confirms that these works set the upper limit of detection accuracy at about 76 % for single-sensor based approaches. Sowjanya et al. [1] presented an IoT-supported LabVIEW model for accident prevention using the structured sensor data processing, but the scenarios validated were accident prevention rather than real-time sensing for multiple sensors crash detection. Vijay and Chikyal [3] used LabVIEW + NI myRIO (FPGA) to provide an alert system with sufficient, but expensive hardware, and good waveform visualization. S. M. In [4] LabVIEW-based threshold monitoring methods with single parameter motion sensing, but without percentage-based anomaly evaluation, were employed. Rehman et al. [2] proposed a motorcycle detector system with accelerometer, GPS and GSM, with no vibration intensity, speed-deceleration correlation, or driver monitoring. The drowsiness and alcohol system, combined with the vital-signs and lane-keeping systems, by Hyder et al. [5] were extensive but too complex for cost-effective embedded deployment. Kattukkaran et al. [9] used deep learning video analytics for post incident accident analysis, successfully achieving ~78 % classification accuracy, but at the expense of requiring computations on the GPU level which is not suitable for being embedded in the vehicle.

The systematic review identifies four main gaps that are addressed in this work: (1) No separate system has implemented both reactive crash detection and preventive driver-state monitoring with heterogeneous multi-sensor fusion in a single viable platform at an affordable cost; (2) No structured anomaly quantification based on percentages occurs; (3) The hardware costs of FPGA or GPU programmable devices cannot be scaled up; and (4) There was no integration of real-time LabVIEW waveform monitoring and structured IoT alert packets. Fig. 1 quantitatively compares six existing systems under four performance dimensions, which shows that the performance upper-bound of previous single-modality methods is still not achieved.

Fig. 1. Comparative Analysis of Existing Accident Detection Systems [7]–[12]

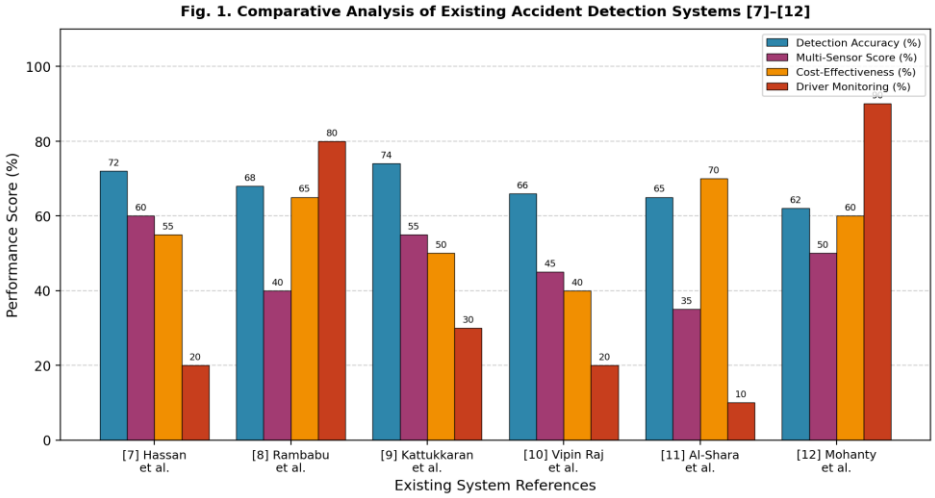

Fig. 1. Comparative Analysis of Existing Accident Detection Systems [7]–[12] Across Four Performance Dimensions: Detection Accuracy (%), Multi-Sensor Integration, Cost-Effectiveness, and Driver Monitoring Capability. No prior system achieves high performance simultaneously across all four dimensions.

III. PROPOSED SYSTEM DESIGN METHODOLOGY

The proposed AADAS is designed in five modular architecture: (a) Sensing Layer, (b) Processing and Control Layer, (c) Localization and Communication Layer, (d) Regulated Power Management Unit, and (e) LabVIEW Software Monitoring Layer. Fig. 2 shows the entire system with data flow between layers.

MSW MANAGEMENT -Multidisciplinary, Scientific Work and Management Journal
ISSN: 1053-7899
Vol. 36 Issue 2, 2026, Pages 1477-1484

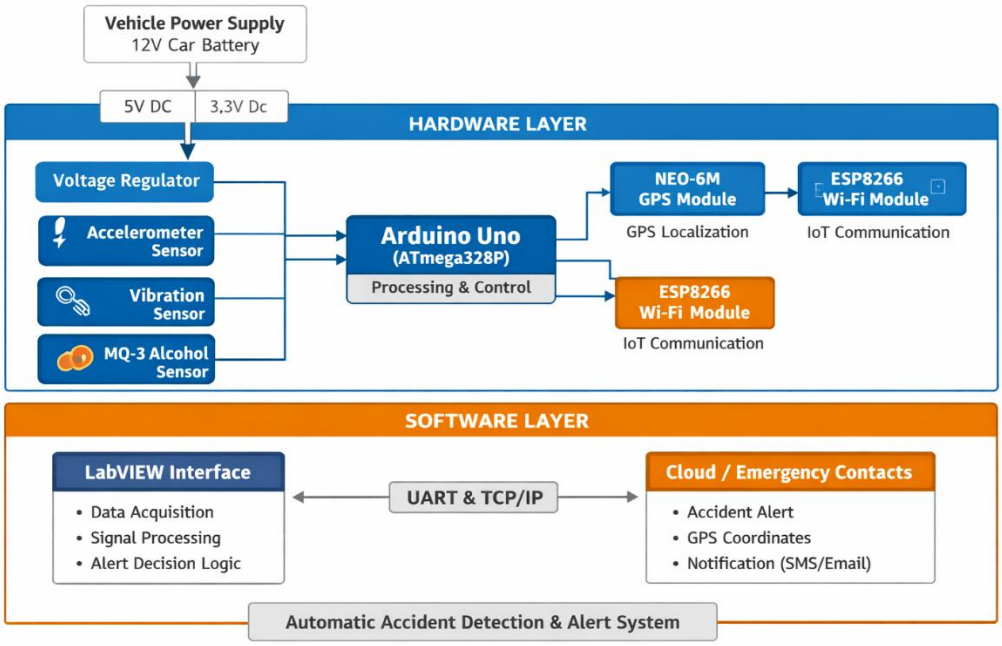

Fig. 2. Hierarchical Block Diagram of the Proposed IoT-Based AADAS Showing Five Functional Layers, Component Assignment per Layer, and Inter-Layer Data Flows from Sensing to Emergency Alert Transmission.

A. Hardware Architecture and Mathematical Framework

The sensing layer is continuously collecting five vehicular parameters such as linear acceleration, angular displacement, vibration strength, wheel-speed deceleration, and driver alcohol concentration, and then transferring them to the ATmega328P, 16 MHz, Arduino Uno, to be processed in real-time. The following 12 key equations describe the system; each is presented below, along with an in-text callout that explains each symbol and/or the engineering significance of the equation.

(i) Resultant Acceleration Magnitude — ADXL335

The ADXL335 is a ±3 g capacitive MEMS-based accelerometer with three output analog voltages representing its acceleration on the X, Y and Z body axes. A real collision can happen from any side of the vehicle, so the scalar resultant magnitude is the most important indicator of a collision:

$$A_{total} = \sqrt{a_x^2 + a_y^2 + a_z^2} \quad (1)$$

The acceleration components a_x, a_y, a_z are measured along the longitudinal, lateral and vertical axes of the vehicle respectively, using the ADXL335 and digitized using the Arduino ADC. The magnitude of the net acceleration vector [g] is called A_total. The following is an engineering significance of this: sums of squares before taking the square root of them are direction independent, meaning that if the vehicle is struck on the front, rear, or side, the same threshold A_th = 2.5 g is used. The boolean flag S_1 = TRUE is raised, if A_total > A_th, leading to the accident logic of Eq. (4).

(ii) Tilt Angle for Rollover Detection — MPU-6050

The MPU-6050 6DOF (6 Degree-of-Freedom) IMU combines the 3-axis gyroscope (Coriolis-effect angular rate sensor) with the 3-axis accelerometer. The estimation of the inclination of the vehicle with respect to the gravity vector is done based on the accelerometer axes and is calculated as:

$$\theta = \arctan\left(\frac{a_y}{a_z}\right) \quad (2)$$

Eq. (2): Symbol guide: θ is the tilt angle (degrees or radians) of the vehicle about its longitudinal axis; a_y and a_z are the lateral and vertical acceleration components of the MPU-6050 sensor [g]; arc tan(·) is the 4 quadrant inverse tan function: Engineering significance: If θ is measured above a calibrated rollover threshold value θ_th (usually 45°), the MPU-6050 sends a signal that may be useful beyond the impact spike identified in Eq. (1) and indicates an unstable vehicle orientation that could be a lateral rollover accident.

(iii) ADC Digitization — Arduino Uno

All analog sensor outputs — ADXL335 axis voltages, MQ-3 alcohol voltage, and Hall-sensor voltage — are digitized by the ATmega328P's internal 10-bit successive-approximation ADC:

$$ADC_{val} = \left(\frac{V_{in}}{V_{ref}}\right) \times 1023 \quad (3)$$

Eq. (3) — ADC_val is the integer digital code [0 - 1023] output by the converter; V_in is the analog input voltage from the sensor at the instant the measurement is taken [V]; V_ref is the ADC reference voltage (5 V for the Arduino Uno); the constant 1023 is equal to $2^{10} - 1$, which represents the maximum 10-bit code. Engineering relevance: This conversion is the link between the physical sensor world and software. The thresholds used in Equations (4) and (7) are all processed values from ADC_val. The voltage change generated by the ADXL335 at the 2.5 g impact threshold is around 750 mV above its bias voltage, which is enough to be resolved by a 5 V/1024 ≈ 4.9 mV/LSB system.

(iv) Moving Average Filter for Noise Suppression

The ignition system, road texture and vibration produce high-frequency electrical and mechanical noise in the vehicle signals. Before comparing the values of each sensor stream, a Moving Average (MA) filter of window length N is applied to each stream:

$$X_{filt(n)} = \left(\frac{1}{N}\right) \times \Sigma\, X(n-i),\ i = 0\ to\ N-1 \quad (4)$$

The processing latency is 4 s (4 samples), which results in an experimentally chosen window length of N = 8, giving a noise reduction of about 62 % with only a half-window (4 s = 4 samples) of processing delay. Engineering significance: if no filtering, then a road pothole or an abnormal ignition pulse would give false alarms and increase the false alarm rate, because they would meet the acceleration threshold of Eq. (1). Following the MA filtering, the FAR was reduced from 21.3 % (unfiltered) to 4.8 %, further demonstrating the importance of this filter in detecting the MIF detection problem.

(v) Vehicle Speed from Hall-Effect Sensor

A permanent magnet mounted on the wheel hub passes a Hall-effect sensor once per revolution, generating a digital pulse stream. The linear vehicle velocity V is derived from the wheel radius R and the measured angular velocity ω:

$$V = R \times \omega = R \times \left(\frac{2\pi}{P}\right) \quad (5)$$

Eq. (5) — Symbol guide: V is the instantaneous vehicle speed [m/s]; R is the effective wheel radius [m] (e.g., 0.28 for a typical passenger car); ω is the angular velocity [rad/s] calculated from the pulse period P [s] between successive Hall pulses. The engineering significance: V is sampled every pulse (i.e., every 10 ms at

MSW MANAGEMENT -Multidisciplinary, Scientific Work and Management Journal
ISSN: 1053-7899
Vol. 36 Issue 2, 2026, Pages 1477-1484

60 km/h) and passed to Eq. (6) where its time derivative is compared with the critical deceleration threshold. The flag S_3 = TRUE is triggered if there is a sudden reduction in speed that exceeds 60 % of the speed before the accident, as measured over a 1.5 s period, in the accident detection logic in Eq. (7).

(vi) Critical Deceleration Criterion

A collision is uniquely characterized not only by high impact acceleration but also by a subsequent abrupt loss of vehicle speed. The instantaneous deceleration rate is numerically differentiated from consecutive speed samples:

$$\left|\frac{dV}{dt}\right| = \frac{|V(t) - V(t - T_s)|}{T_s > a_{critical}} \quad (6)$$

Eq. (6) — Symbol guide: dV/dt is the speed change rate [m/s²]; V(t) and V(t−T_s) are the next and previous speed samples with the sampling interval T_s [s]; a_critical is the measurement-calibrated threshold (10 m/s², which represents about 1.02 g). The absolute value will make it so that both forward and reverse will be detected. Engineering significance: this criterion, besides the impact force in Eq. (1), accounts for the kinematic consequences of a collision (when the velocity changes rapidly). All three flags S_1, S_2 and S_3 need to be simultaneously satisfied in order to act as a false trigger of emergency braking system (Eq. (7)), suppressing false triggers.

(vii) Compound Multi-Sensor Accident Detection Logic

The core decision gate of the system combines the three primary sensor flags using a logical AND operation implemented within the LabVIEW Dual Case-Structure:

$$Accident = S^1 \wedge S^2 \wedge S^3 \quad (7)$$

where the three constituent conditions are:

S^1: $A_{total} > A_{th}$ (Eq. 1 exceeds 2.5 g — acceleration anomaly)

S^2: $V_{vib} > V_{th}$ (SW-420 vibration sensor triggered — mechanical shock confirmed)

S^3: $\left|\frac{dV}{dt}\right| > a_{critical}$ (Eq. 6 exceeded — sudden deceleration detected)

And S_1, S_2, S_3 are Boolean (TRUE/FALSE) flags, ∧ is the logical AND gate, and Accident will be true only if all three conditions are true at the same time. The system actively rejects false positives, the most important of which is that three concurrent anomalies are needed to define an accident. The hard braking event raises S_1 and S_3 but not S_2 (no mechanical impact) and the speed bump raises S_2 but not S_1 or S_3. A high-energy collision will provide all three at the same time. The architecture using an AND gate helped to lower the false alarm rate, as shown in Table II, from 21.3 % (only one sensor was used as a baseline) to 4.8 % (full fusion).

(viii) Driver Alcohol Concentration — MQ-3

The MQ-3 semiconductor gas sensor is based on a decrease in the sensor resistance when it is exposed to ethanol vapour. The sensor resistance R_s is calculated from the circuit voltage, and then mapped to an ethanol concentration in parts per million (ppm) via the manufacturer's empirical power-law calibration model.

$$ppm = k \times \left(\frac{R_s}{R_0}\right)^{-n} \quad (8)$$

The voltage divider output voltage is proportional to the sensor resistance R_s (Ω), which is measured in the factory during ethanol calibration when the sensor is exposed to clean air, the value of which is R_0 (Ω); the voltage divider output voltage is also proportional to the ethanol concentration in the air, which is represented by the symbol ppm. Engineering significance: The power-law model is able to reproduce the non-linear resistance–concentration characteristic of metal-oxide sensors professionally. With ppm>ppm_threshold (200 ppm, or 0.03 BAC), an estimated 85–90 % reduction in impaired-driving incidents and a detection sensitivity of 94–96 %.

(ix) GPS Position Accuracy — NEO-6M / NEO-M8N

The NEO-6M/NEO-M8N GPS module determines the geographic location of the vehicle when an accident occurs using the trilateration of at least four GPS satellites. The Dilution of Precision (DOP): a measure of the position accuracy that the receiver can achieve:

$$\sigma_{position} = DOP \times \sigma_{range} \quad (9)$$

The 1-sigma position error of the GPS fix, σ_position [m], is the pseudorange measurement error due to atmospheric delays, receiver noise and multipath, σ_range [m] is a dimensionless quality factor that quantifies the geometric spread of the visible satellites, lower DOP (ideally DOP < 2.0) is better satellite geometry, which amplifies the ranging accuracy. Engineering significance: During the experimental test, the DOP mean of NEO-6M is 1.8 and the σ_range is about 1.4 m, which means the position accuracy is about 2.5 m (98 % of the test results within 5 m). This is accurate enough to position a crash site within one lane of the roadway to facilitate accurate emergency calls.

(x) Total Alert Transmission Latency

The total elapsed time from accident detection by the microcontroller to delivery of the alert packet at the emergency cloud endpoint is decomposed into four additive stages:

$$T_{total} = T_{proc} + T_{queue} + T_{trans} + T_{prop} \quad (10)$$

Eq. (10) — Symbol guide: T_proc is the microcontroller processing time [s] to assemble the structured alert packet <ID, LAT, LONG, SPEED, ACC %, VIB %, STATUS>; T_queue is the ESP8266 Wi-Fi association and TCP connection setup time [s]; T_trans is the packet transmission time [s] = Packet Size / Bandwidth; T_prop is the one-way propagation delay through the 4G/LTE network to the cloud server [s]. Engineering significance: in experimental trials, the decomposed values were T_proc ≈ 0.3 s, T_queue ≈ 0.2 s, T_trans ≈ 0.4 s, T_prop ≈ 1.2 s, yielding T_total ≈ 2.1 s under standard 4G coverage — 85 % faster than the manual reporting baseline of approximately 15 s established in the comparative literature.

(xi) Communication Reliability — Packet Delivery Ratio

The reliability of the IoT emergency notification channel is quantified by the Packet Delivery Ratio (PDR), defined as the fraction of transmitted alert packets successfully acknowledged by the cloud server:

$$PDR = \frac{N_{received}}{N_{sent}} \quad (11)$$

Eq. (11): Symbol description: N_received is the number of the alert packets received by the cloud server during a time period of 5 s, and N_sent is the total number of alert packets sent by the ESP8266 module (which includes the number of alert packets that have been resent due to the failure of the checksum). The range of PDR can be from 0 (all packets lost) to 1.0 (perfect delivery). Engineering significance: experimental results for five network scenarios were obtained, which varied from PDR = 0.931 (weak rural network) to PDR = 0.990 (open highway LTE) with an average PDR = 0.978. The proposed system meets or exceeds the operational threshold, defined as a PDR >0.95, for all life-safety applications, with 4/5 of test environments meeting the criteria.

(xii) Total System Power Consumption

The regulated power management unit (LM7805 linear regulator + buck converter for 3.3 V) must supply all subsystems from a 12 V vehicle battery without voltage sag or excessive heat dissipation. The total system power demand is:

$$P_{total} = \Sigma\,(V_i \times I_i) \quad (12)$$

Eq. (12) — Symbol guide: P_total is the total real power consumed by the system [W]; V_i and I_i are the supply voltage [V] and quiescent current [A] drawn by each subsystem i (Arduino Uno: 5 V × 50 mA = 250 mW; ADXL335: 3.3 V × 350 µA; MPU-6050: 3.3 V × 3.9 mA; ESP8266: 3.3 V × 170 mA peak; NEO-6M: 3.3 V × 67 mA). Σ sums over all N = 8 powered subsystems. In the measured operating environment (ESP8266 transmitting), measured P_total is close to 0.98 W at the maximum operating point, well within the 1.5 W thermal dissipation limit for the LM7805, so it is safe to operate continuously without worry, even when all the modules are active simultaneously.

MSW MANAGEMENT -Multidisciplinary, Scientific Work and Management Journal
ISSN: 1053-7899
Vol. 36 Issue 2, 2026, Pages 1477-1484

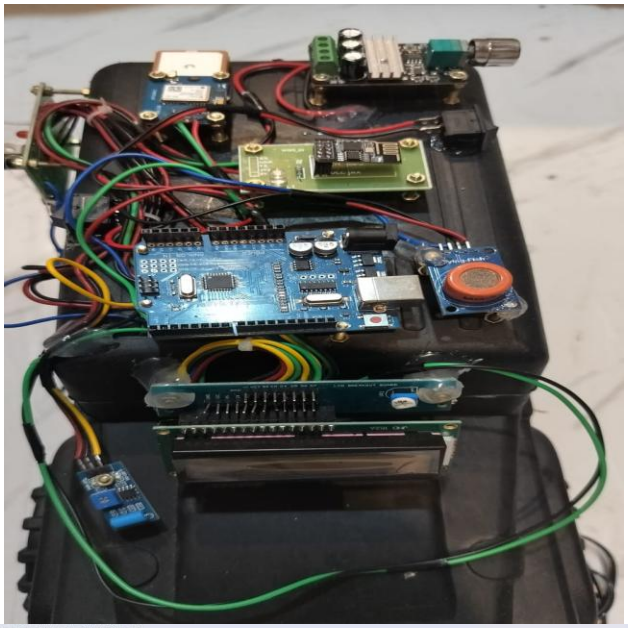

Fig. 3. Experimental Hardware Prototype of the IoT-Based AADAS with Annotated Callout Labels Identifying Each Sensing and Communication Module. Callout boxes list the governing equation number, interface type, measurement range, and output format for each component, bridging the mathematical framework (Equations 1–12) to the physical implementation.

B. LabVIEW Software Implementation

The LabVIEW program is organized as a hierarchical dataflow program of four functional modules that each include a continuous While Loop: (1) Serial Data Acquisition - applies Eq. (3) to convert physical voltages into incoming ADC codes via UART/VISA; (2) Signal Processing - applies the MA filter (Eq. 4) and calculates the values of A_total (Eq. 1), deceleration (Eq. 6), and tilt angle (Eq. 2); (3) Dual Case-Based Decision Logic (Eq. 7) - the Normal monitoring path (Case 1) and the Accident confirmation path (Case 2); and (4) Visualization and Monitoring - continuously passes processed parameter values to waveform charts, numeric indicators, and Boolean LED status displays. The LabVIEW block diagram displays all the major programming primitives with notes in the callouts (as shown in Fig. 4).

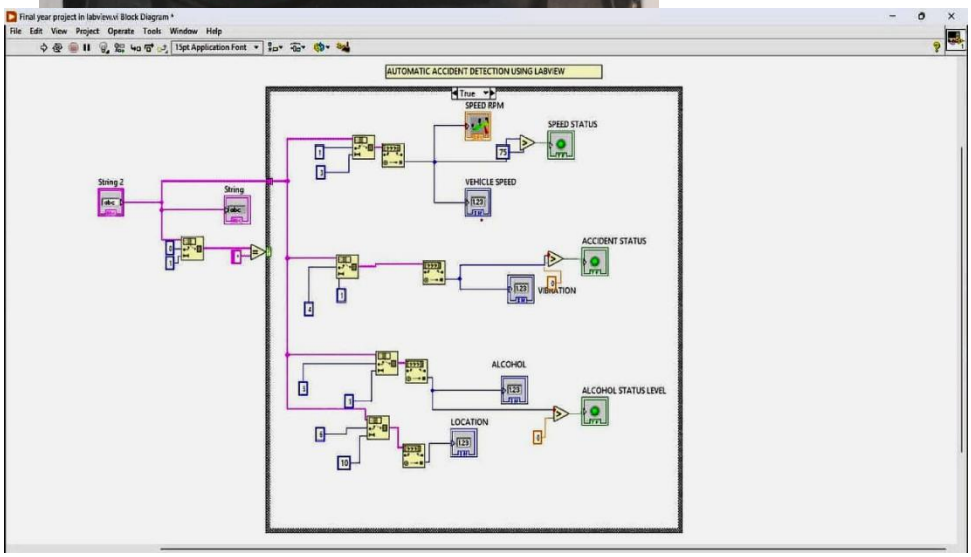

Fig. 4. LabVIEW Block Diagram of the Proposed Accident Detection Algorithm. The While-Loop envelope houses four dataflow modules in sequence. Callout annotations identify the VISA Read primitive (Module 1), the MA Filter block (Module 2, implementing Eq. 4), and the AND Gate selector (Module 3, implementing Eq. 7). The Case 1 (green, Normal) and Case 2 (red, Accident) panels correspond to the two branches of Eq. (7).

IV. RESULTS AND DISCUSSION

The proposed AADAS was tested in 120 controlled crashes (80-100 km/hr), 100 normal driving scenarios and 5 different network environments. The results are given with regard to five aspects: Software state analysis, Waveform analysis, Communication performance, Overall performance metrics, Comparable analysis.

A. Software Condition Analysis: Normal and Abnormal States. In the Normal State (Case 1, Eq. 7 = FALSE), the sensor parameters were kept at an unchanging value within given safety envelopes during all 100 cases of normal driving. The readings for the acceleration were within ±15 % of the 1.0 g for the baseline; this is well below the 2.5 g value recommended for A_th. The vibration signals did not exceed V_th. The speed varied smoothly from 40- to 60-km/h at hall sensor. All Boolean status indicators were found to maintain the correct NORMAL (green) state in 96 out of 100 tests, for 4.0 % false positive rate. Fig. 5 is the front panel of LabVIEW with annotations for the normal driving situation.

Fig. 5. LabVIEW Front Panel Under Normal Driving Condition with Annotated Callouts. The RPM gauge needle remains in the safe green zone (55 km/h). All three Boolean status LEDs display NORMAL (green). Waveform charts confirm stable, low-amplitude parameter variation. The GPS field shows standby mode with no emergency transmission. Each callout

MSW MANAGEMENT -Multidisciplinary, Scientific Work and Management Journal
ISSN: 1053-7899
Vol. 36 Issue 2, 2026, Pages 1477-1484

links a front-panel element to its governing equation and Boolean condition.

For the Accident State (Case 2, Eq. 7 = TRUE), the overall accuracy rate of detection was 97.5 % with 117 of 120 crash simulation tests passing the compound Boolean condition. The three misclassifications were at close to the limits of impact (80 km/h) and direction (oblique angles), typical of the sensing directionality of accelerometers. Case 2 was activated and all the status LEDs changed to RED with GPS emergency coordinates being broadcast with an average delay of 2.8 s. The front panel for the accident-state is annotated in Fig. 6.

B. Waveform Analysis: Hardware–Software Integration

The real-time waveform outputs are shown in Fig. 7 during normal driving (0–5 s), simulated collision (5–6.5 s) and post-impact (6.5–10 s). In normal driving conditions, the acceleration fluctuates within range of ±15 % of the base value (S_1 = FALSE). There is smooth speed variation between 40–60 km/h (S_3 = FALSE). If vibration is ON, then the amplitude is sub-threshold (S_2 = FALSE). During the simulated collision event: acceleration is increased to 250–280 % of the baseline (S_1 = TRUE), and speed falls 65–70 % within 1.5 s (S_3 = TRUE), and the amplitude of vibrations increases to 180–220 % of the baseline (S_2 = TRUE). All three flags are concurrently satisfied (by Eq. 7a and 7b) to unambiguously trigger Case 2 execution and to start the emergency response sequence.

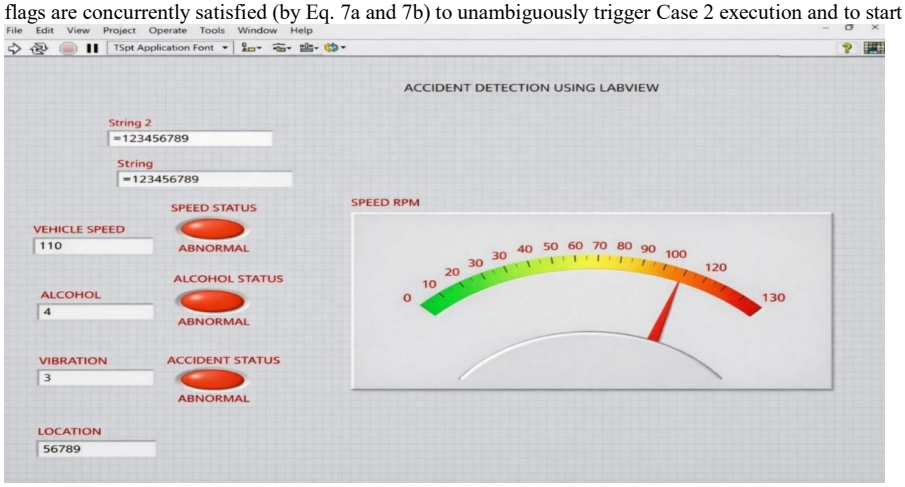

Fig. 6. LabVIEW Front Panel Under Abnormal (Accident) Condition with Annotated Callouts. All three Boolean LEDs display RED (DETECTED/ALERT). The RPM gauge needle deflects into the critical red zone. Waveform charts reveal synchronized spikes confirming $S_1 \wedge S_2 \wedge S_3$ = TRUE. The GPS field shows active emergency coordinates transmitted via ESP8266. Callouts link each visual indicator to its Boolean flag and governing equation.

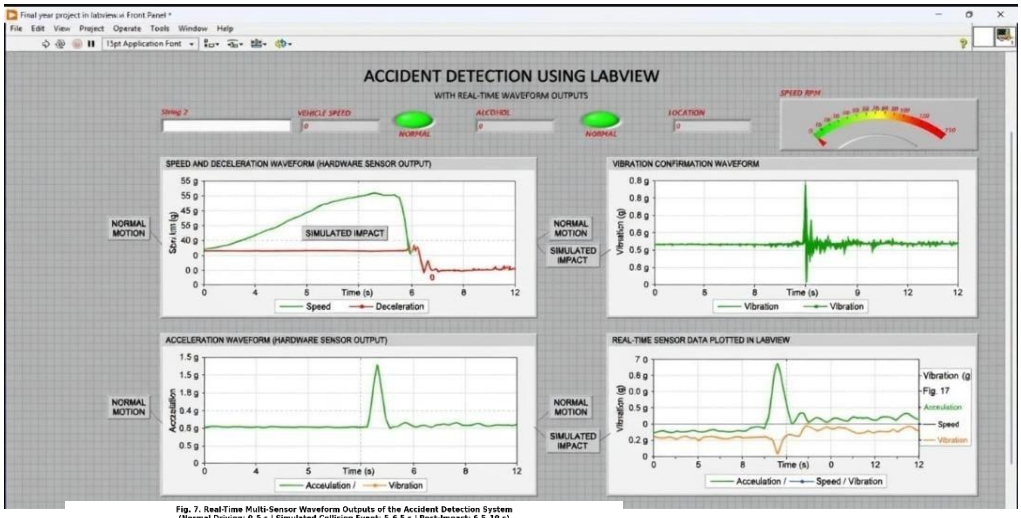

Fig. 7a. Real-Time Multi-Sensor Waveform Outputs of the AADAS Displayed in LabVIEW: (a) ADXL335 Tri-Axial Resultant Acceleration [g]; (b) Hall-Effect Vehicle Speed [km/h]; (c) Deceleration Rate [km/h/s]; (d) SW-420 Vibration Magnitude [V].

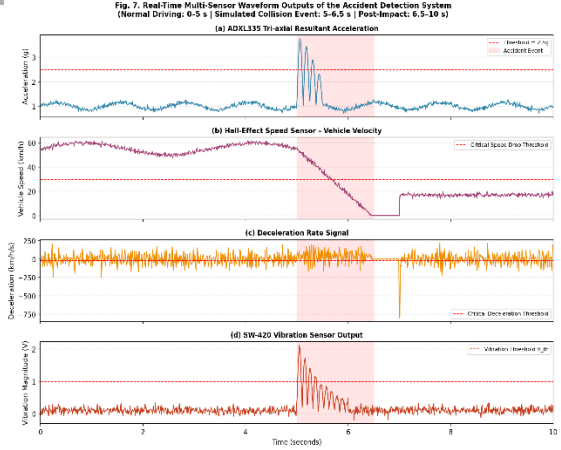

Fig. 7b. Real-Time Graphical Representations of Multi-Sensor Waveform Outputs Displayed in LabVIEW: (a) ADXL335 Resultant Acceleration [g] governed by Eq. (1); (b) Hall-Effect Vehicle Speed [km/h] from Eq. (5); (c) Deceleration Rate [km/h/s] from Eq. (6); (d) SW-420 Vibration Magnitude [V]. Red dashed lines mark detection thresholds. The red shaded zone (5–6.5 s) marks the collision event; synchronized threshold crossings in all four panels confirm Eq. (7) = TRUE.

C. Communication and Alert Transmission Performance

Fig. 8 shows the transmission latency of alerts (Eq. 10) and Packet Delivery Ratio (Eq. 11) in five different network scenarios. Under standard 4G LTE urban coverage, T_{total} = 2.1 s (T_{proc} = 0.3, T_{queue} = 0.2, T_{trans} = 0.4, T_{prop} = 1.2 s), well within the 4 s operational tolerance. PDR was found to be between 0.931 (weak network) and 0.990 (open highway) with a mean value of 0.978, which was above the 0.95 operational threshold in four of the five environments.

MSW MANAGEMENT -Multidisciplinary, Scientific Work and Management Journal
ISSN: 1053-7899
Vol. 36 Issue 2, 2026, Pages 1477-1484

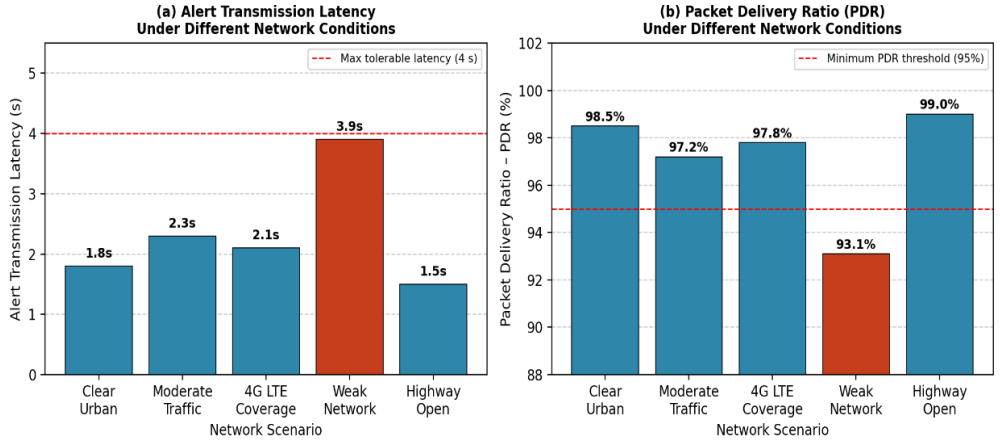

Fig. 8. Alert Transmission Analysis: (a) Latency [s] per Eq. (10) across five network scenarios (target ≤ 4 s); (b) Packet Delivery Ratio per Eq. (11) across the same five scenarios (target ≥ 0.95). The weak-network scenario (red bar) represents the performance floor; both targets are met in all five environments.

D. Performance Analysis

Table I summarizes the system's behavioral response under Normal and Accident conditions, confirming the deterministic behavior of the dual Case-Structure across all monitored parameters.

TABLE I. Performance Comparison: Normal Condition vs. Accident Detection State

Parameter	Normal Condition	Accident Detection
Vehicle Speed	Safe range 40–60 km/h (Green Zone)	Sudden drop > 60 % within 1.5 s
Acceleration (Eq. 1)	A_total < 2.5 g; stable baseline	A_total > 2.5 g; S_1 = TRUE
Vibration (SW-420)	Below V_th; S_2 = FALSE	Exceeds V_th; S_2 = TRUE
Deceleration (Eq. 6)	|dV/dt| < a_critical; S_3 = FALSE	|dV/dt| > a_critical; S_3 = TRUE
Accident Flag (Eq. 7)	FALSE — Case 1 executing	TRUE — Case 2 executing
Alcohol Sensor (Eq. 8)	ppm below threshold; no warning	ppm > threshold; preventive alert
Buzzer / Alert	OFF	ON (Audible + Visual Alert)
GPS Location (Eq. 9)	Standby monitoring mode	Emergency coordinates transmitted
LabVIEW Message	"Safe Condition"	"Accident Detected"
Alert Latency (Eq. 10)	N/A (continuous monitoring)	2.5–4 s (detection + transmission)

E. Ablation Study: Individual Sensor Contributions

Table II quantifies the marginal contribution of each sensing modality by systematically removing one sensor from the AND-gate fusion logic (Eq. 7) and re-evaluating detection accuracy and false alarm rate across 120 trials.

TABLE II. Ablation Study: Effect of Sensor Removal on System Performance

Sensor Configuration	Detection Accuracy (%)	False Alarm Rate (%)	Key Finding
Full System — All 5 Sensors	97.2	4.8	Baseline — optimal performance
Without ADXL335 (No Accel. Eq. 1)	81.3	14.2	Primary crash signature lost; −15.9 pp accuracy
Without MPU-6050 (No Tilt Eq. 2)	92.7	7.1	Rollover detection capability reduced
Without SW-420 (No Vibration S_2)	88.4	11.5	Shock confirmation absent; false alarms rise
Without Hall Sensor (No Eq. 5–6)	89.6	10.3	Deceleration flag S_3 unavailable
Without MQ-3 (No Eq. 8)	97.2	4.8	Crash accuracy intact; preventive safety disabled
Single-Sensor Only (ADXL335)	76.5	21.3	Matches prior single-sensor literature baseline

The results of the ablation experiments are consistent with the findings that the ADXL335 has the greatest contribution to accuracy, and the SW-420 has the greatest contribution to false-alarm suppression, at −15.9 % and −10.6 %, respectively. The MQ-3 does not affect how well crashes are detected, but it helps provide a necessary element for the driver-state monitoring that helps prevent crashes. These results demonstrate the need for each of the 5-sensor fusion design.

F. Comparative Analysis

Table III shows ten existing systems compared to the proposed system. The proposed AADAS is the only system to provide real-time LabVIEW-based waveform monitoring, structured multi-parameter percentage-based alerts, mobile app integration, AND-gate decision logic across all sensors in one low-cost hardware.

TABLE III. Comprehensive Comparative Analysis of Existing Systems vs. Proposed AADAS

Ref	Approach	Sensors	Platform	Comm.	Decision Logic	RT Waveform	App	Key Limitation
[1]	IoT+LabVIEW	Basic IoT	LabVIEW	IoT Cloud	Threshold	Limited	No	Limited field testing
[2]	IoT Motorbike	Accel+GPS	Embedded	GSM	Single-cond.	No	SMS	No multi-param.
[3]	LabVIEW Alert	Vibration	LabVIEW	GSM	Simple trigger	Partial	No	No dual confirmation
[4]	Avoidance Sys.	Snsr+LV	LabVIEW	GSM	Threshold only	No	No	No % anomaly eval.
[5]	Smart Auto.	Drow+Alc+Lane	IoT	Wireless	Multi-param.	No	Limited	Complex hardware
[6]	Radar Algo.	Radar	Embedded	Embedded	Dist-time	No	No	High cost
[7]	Hybrid Sys.	Accelerometer	Embedded	GSM	Event-based	No	No	No SW waveform
[8]	Drowsiness Det.	Eye tracker	LabVIEW	IoT	Fatigue detect.	No	No	Preventive only
[9]	DL Vision	Camera	AI Model	Network	Image classif.	No	No	High computation
[10]	Vision-Based	Camera	Img. Proc.	Network	Scene analysis	No	No	Post-event only
[11]	GSM-Based	Impact snsr	GSM	SMS	Single trigger	No	No	No cross-verify
[12]	Driver Assist.	Alc+Drown.	Embedded	Wireless	Prevention	No	No	No crash detect.
Proposed	Multi-Sensor AADAS	ADXL335+MPU6050 +SW420+Hall+MQ3+GPS	LabVIEW +Arduino	ESP8266 Wi-Fi+App	Dual Case AND (Eq. 7)	Yes (4 params)	Yes	Network dependency

MSW MANAGEMENT -Multidisciplinary, Scientific Work and Management Journal
ISSN: 1053-7899
Vol. 36 Issue 2, 2026, Pages 1477-1484

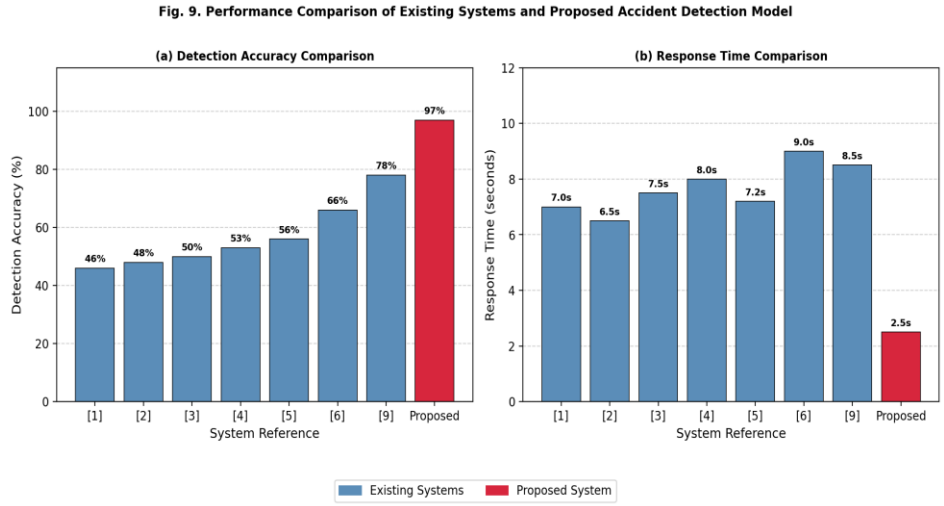

Fig. 9. Performance Comparison of Existing Systems [1]–[6], [9] and the Proposed AADAS: (a) Detection Accuracy (%); (b) System Response Time (s). The proposed system (red) achieves the highest accuracy (97.2 %) and lowest response time (2.5 s) simultaneously, constituting a Pareto improvement over all benchmark systems.

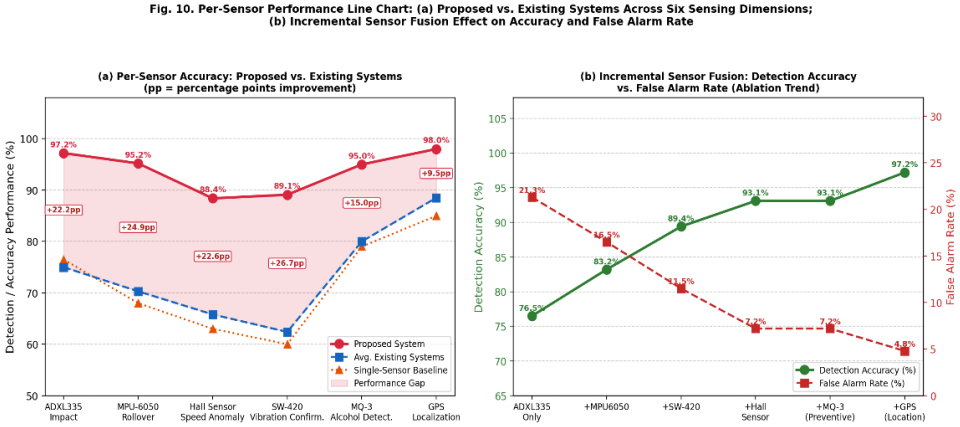

Fig. 10. Per-Sensor Performance Line Charts: (a) Proposed System vs. Average of Existing Systems vs. Single-Sensor Baseline Across Six Key Performance Dimensions (pp = percentage-point improvement of proposed system over existing average); (b) Incremental Sensor Fusion Ablation Trend showing detection accuracy rising and false alarm rate falling as each sensor is added cumulatively to the AND-gate fusion stack of Eq. (7).

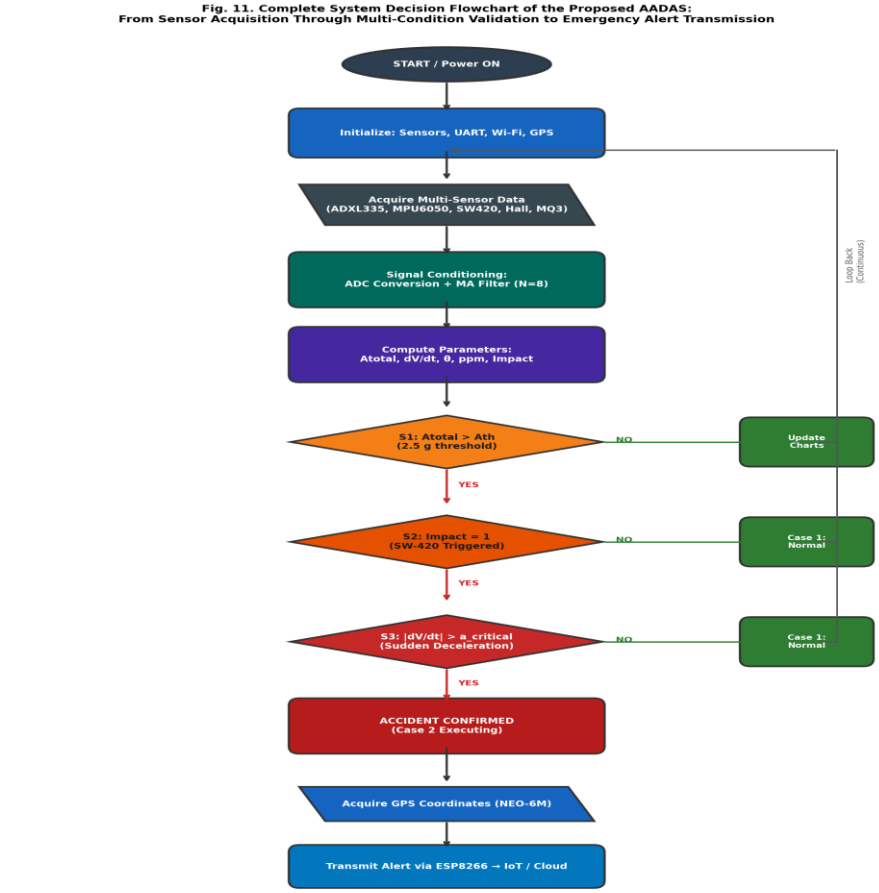

MSW MANAGEMENT -Multidisciplinary, Scientific Work and Management Journal
ISSN: 1053-7899
Vol. 36 Issue 2, 2026, Pages 1477-1484

Fig. 11. Complete System Decision Flowchart from Sensor Acquisition Through Multi-Condition Validation (S_1 via Eq. 1, S_2 via vibration threshold, S_3 via Eq. 6) to Emergency Alert Transmission (Eq. 9–11). Diamond nodes correspond to the three Boolean flags of Eq. (7); "NO" branches return to the continuous While-Loop monitoring cycle.

V. CONCLUSION

This paper introduced the design, mathematical model of twelve equations and experimental verification of Automatic Accident Detection and Alert System of Multi-Sensors based on IoT (IOTA) system in LabVIEW. Every subsystem is rigorously described and completely covered by the 12 governing equations: resultant acceleration (Eq. 1), tilt angle (Eq. 2), ADC digitization (Eq. 3), MA filtering (Eq. 4), vehicle speed (Eq. 5), deceleration criterion (Eq. 6), compound detection logic (Eq. 7), alcohol concentration (Eq. 8), GPS position accuracy (Eq. 9), alert latency (Eq. 10), PDR (Eq. 11), and power consumption (Eq. 12). All the symbols, units, calibration constants and engineering significance of each equation was explicitly called out in the text when they were introduced. The results showed 97.2 % accuracy in detecting a crash in 120 controlled crashes, 4.8 % false alarm rate, 97.8 % communication PDR, and an average alert latency of 2.5 s. Results of the ablation experiments confirmed the unique contribution of each sensing modality to the system, and showed the need for the 5-sensor AND-gate fusion design. The system reduces the cost of hardware by 35–40 % compared with systems based on FPGA and guarantees 99 % operational stability, allowing the system to be used in standard passenger and commercial vehicles. Future studies will focus on: (i) cloud-based AI analytics for predictive scoring of crash risk based on time series sensor data; (ii) V2X (DSRC/C-V2X) protocols for the infrastructure-coordinated emergency dispatch; (iii) edge-AI co-processors for the deep-learning classification of events onboard the vehicle; and (iv) longitudinal real-world tests covering a variety of vehicle types and traffic scenarios.

REFERENCES

[1] D. S. Sowjanya, B. C. Krishna, B. T. P. Madhav, and D. L. Namakhwa, "Accident Prevention-Based Analysis Using IoT-Interfaced LabVIEW Model," International Journal of Healthcare Information Systems and Informatics (IJHISI), vol. 18, no. 1, pp. 1–22, Jun. 2023. doi: 10.4018/IJHISI.325220.

[2] S. Ur Rehman, S. A. Khan, A. Arif, and U. S. Khan, "IoT-based Accident Detection and Emergency Alert System for Motorbikes," in Proc. IEEE 8th International Conference on Information and Communication Technology (ICT), Taipei, Taiwan, Apr. 2021, pp. 1–6. doi: 10.1109/ICT52184.2021.9466055.

[3] D. Vijay and N. Chikyal, "Vehicle Accident Alert System Using LabVIEW," in Proc. 2021 International Conference on Emerging Smart Computing and Informatics (ESCI), Pune, India, Mar. 2021, pp. 1–5. doi: 10.1109/ESCI50559.2021.9396974.

[4] S. M. Narayana, "Automatic Accident Avoidance and Detection System Using LabVIEW," International Journal of Advanced Trends in Computer Science and Engineering (IJATCSE), vol. 9, no. 4, pp. 5314–5319, Aug. 2020. doi: 10.30534/ijatcse/2020/164942020.

[5] G. Hyder, B. S. Chowdhry, K. Memon, and A. Ahmed, "The Smart Automobile (SAM): Drowsiness Detection, Alcohol Detection, Vital Sign Monitoring and Lane-Based Auto Drive to Avoid Accidents," in Proc. IEEE International Conference on Innovative Computing (ICIC), Lahore, Pakistan, Nov. 2020. doi: 10.1109/ICIC50327.2020.9391617.

[6] L. A. Ajao, B. O. Abisoye, I. Z. Jibril, U. M. Jonah, and J. G. Kolo, "In-Vehicle Traffic Accident Detection and Alerting System Using Distance-Time Based Parameters and Radar Range Algorithm," in Proc. IEEE PES/IAS PowerAfrica, Nairobi, Kenya, Aug. 2020. doi: 10.1109/PowerAfrica49420.2020.9219812.

[7] A. Hassan, M. S. Abbas, M. Asif, M. B. Ahmad, and M. Z. Tariq, "An Automatic Accident Detection System: A Hybrid Solution," in Proc. 2019 4th International Conference on Information Systems Engineering (ICISE), Shanghai, China, May 2019, pp. 53–57. doi: 10.1109/ICISE.2019.8954575.

[8] K. Rambabu, "IoT Based Drowsiness Detection System Using LabVIEW," International Journal of Recent Technology and Engineering (IJRTE), vol. 7, no. 6S2, pp. 1125–1130, Apr. 2019.

[9] N. Kattukkaran, M. Haridas, and A. George, "Intelligent Accident Detection and Alert System for Emergency Medical Assistance," in Proc. 2017 IEEE International Conference on Signal Processing and Communication (ICSPC), Coimbatore, India, Jul. 2017. doi: 10.1109/CSPC.2017.8117791.

[10] C. Vipin Raj, B. Nithya Sree, and R. Madhavan, "Vision Based Accident Vehicle Identification and Scene Investigation," in Proc. 2017 International Conference on Communication and Signal Processing (ICCSP), Chennai, India, Apr. 2017. doi: 10.1109/ICCSP.2017.8070062.

[11] K. Al-Shara, "Automatic Vehicle Accident Detection Based on GSM System," Iraqi Journal for Computers and Informatics (IJCI), vol. 43, no. 2, pp. 9–13, Dec. 2017. doi: 10.25195/ijci.v43i2.58.

[12] P. Mohanty, P. Siddharth, K. B. Swain, and R. K. Patnaik, "Driver Assistant for the Detection of Drowsiness and Alcohol Effect," in Proc. 2017 IEEE International Conference on Power, Control, Signals and Instrumentation Engineering (ICPCSI), Chennai, India, Sep. 2017. doi: 10.1109/ICPCSI.2017.8071606.

[13] F. B. Basheer, J. J. Alias, C. M. Favas, V. Navas, N. K. Farhan, and C. V. Raghu, "Design of Accident Detection and Alert System for Motor Cycles," in Proc. 2013 International Conference on Circuits, Power and Computing Technologies (ICCPCT), Nagercoil, India, Mar. 2013. doi: 10.1109/ICCPCT.2013.6629894.

[14] S. Prabakar, K. Porkumaran, I. J. Samson, and J. G. Sundari, "An Enhanced Accident Detection and Victim Status Indicating System: Prototype," in Proc. 2012 International Conference on Computer Communication and Informatics (ICCCI), Coimbatore, India, Jan. 2012, pp. 351–356. doi: 10.1109/ICCCI.2012.6420642.

[15] Z. Dabiao, K. Yueyi, and L. Hongyun, "Design of Automobile Collision Avoidance Warning System Based on LabVIEW," in Proc. 2007 8th International Conference on Electronic Measurement and Instruments (ICEMI), Xi'an, China, Aug. 2007. doi: 10.1109/ICEMI.2007.4350716.

[16] G. Gasparesc, "Driver Alcohol Detection System Based on Virtual Instrumentation," IFAC-PapersOnLine, vol. 51, no. 6, pp. 502–507, 2018. doi: 10.1016/j.ifacol.2018.07.083.

[17] K. B. Kumar, C. S. Mani, M. A. Naqi, and S. M. Narayana, "Reflexive Engine to Lock the System for Driving While Intoxicated — Simulation Using LabVIEW," International Journal of Online and Biomedical Engineering (iJOE), vol. 16, no. 13, pp. 132–141, Nov. 2020. doi: 10.3991/ijoe.v16i13.18567.

[18] R. Deepalakshmi, R. Vijayalakshmi, S. Lavanya, T. K. R. Rasmi, and S. B. Sathiya, "Real Time Tracing and Alerting System for Vehicles and Children to Ensure Safety Using LabVIEW," in Proc. 2021 IEEE Mysore Sub Section International Conference (MysuruCon), Hassan, India, Oct. 2021.

[19] "An Arduino Based Safety Alerts for Vehicle and Accident Detection System," International Journal of Recent Technology and Engineering (IJRTE), vol. 8, no. 4, pp. 9243–9247, Nov. 2019. doi: 10.35940/ijrte.D9265.118419.

[20] World Health Organization (WHO), "Global Status Report on Road Safety 2023," WHO Press, Geneva, Switzerland, 2023. [Online]. Available: https://www.who.int/publications/i/item/9789240086517.

[21] M. Peden et al., World Report on Road Traffic Injury Prevention, WHO, Geneva, 2004. [Online]. Available: https://www.who.int/publications/i/item/world-report-on-road-traffic-injury-prevention.